International Journal of Technology 13(8) 1663-1671 (2022)
Received September 2022 / Revised November 2022 / Accepted December 2022

International Journal of Technology

http://ijtech.eng.ui.ac.id

Design of a Transforaminal Lumbar Interbody Fusion (TLIF) Spine Cage

Afrah Faadhila[1], Siti Fauziyah Rahman[1,2], Yudan Whulanza[2,3]*, Sugeng Supriadi[2,3], Joshua Yoshihiko Tampubolon[4], Septian Indra Wicaksana[4], Ahmad Jabir Rahyussalim[5], Tri Kurniawati[6], Abdul Halim Abdullah[7]

[1]Biomedical Engineering Study Program, Department of Electric Engineering, Faculty of Engineering, Universitas Indonesia, Kampus UI Depok, West Java 16424, Indonesia
[2]Research Center for Biomedical Engineering, Faculty of Engineering, Universitas Indonesia, Kampus UI Depok, West Java 16424, Indonesia
[3]Department of Mechanical Engineering, Faculty of Engineering, Universitas Indonesia, Kampus UI Depok, West Java 16424, Indonesia
[4]PT Trafas Dwi Medika, Jakarta 13920, Indonesia
[5]Department of Orthopaedic and Traumatology, Cipto Mangunkusumo National Central General Hospital and Faculty of Medicine, Universitas Indonesia, Jakarta 10430, Indonesia
[6]Stem Cell and Tissue Engineering Cluster, Indonesian Medical Education and Research Institute, Faculty of Medicine, Universitas Indonesia, Jakarta 10430, Indonesia
[7]Biomechanical & Clinical Engineering Research Group, College of Engineering, Universiti Teknologi Mara, Malaysia

Abstract. Lumbar Interbody Fusion is a technique used to treat various spinal disorders, which has many types, such as the Transforaminal Lumbar Interbody Fusion (TLIF) Technique. With TLIF being one of the most well-known techniques, which many spinal surgeons are trained and skilled at, there are various types of TLIF Spine Cages available on the market. In this paper, we designed a TLIF Cage and compared the simulation's analysis with the prototype's experimental testing. The design was developed using the reverse engineering method, and findings on the jaws profile and other design considerations through literature review. The design was then analyzed through a simulated compression test using Ansys Software. The simulation showed that the designed TLIF spine cage in this paper can withstand the force usually given to an implanted lumbar spinal cage.

Keywords: 3D Design; Interbody Fusion; Spine Cage; TLIF implant

1. Introduction

Patients increasingly suffer spinal injuries due to accidents or incorrect movement positions in athletes. The loss or reduced function of the spinal disc to support the spine and maintain foraminal height is one of the most common injuries. This injury can cause the narrowing of the spinal canal, or degenerative lumbar spinal stenosis, which affects the patient's movement (Lee *et al.,* 2020). If not properly treated, this disease can lead to ischemia and chronic pain (Lee *et al.,* 2020). Several types of treatment can be given to patients, ranging from therapeutic testing with injections for minor injuries, combining medications with physical therapy, for spine cage implant surgery using the lumbar interbody fusion technique (Hennemann & de Abreu, 2021; Mobbs *et al.,* 2015). The

*Corresponding author's email: yudan.whulanza@ui.ac.id, Tel.: +62-217270032, Fax.: Tel.: +62-217270033
doi: 10.14716/ijtech.v13i8.6152

Lumbar Interbody Fusion Technique treats various spinal disorders, including degenerative pathologies, trauma, infection, and neoplasia. This technique is done by inserting an implant, a cage, a spacer, or a structural graft, into the intervertebral space using various approaches (Mobbs *et al.*, 2015).

There are several spine cage implant options available that differ in their geometry depending on the approach for insertion. First is Posterior Lumbar Interbody Fusion (PLIF) which many spinal surgeons are well-trained to use. It provides better nerve root visualization than other cages. But it also requires high neural retraction. Then there is Anterior Lumbar Interbody Fusion (ALIF) as the most efficacious and predominant treatment for discogenic low back pain which can maximize implant size and surface area. But ALIF insertion surgery can cause some complications, such as retrograde ejaculation, and visceral and vascular injury. For sagittal and coronal deformity correction, lateral lumbar interbody fusion (LLIF) and oblique lumbar interbody fusion (OLIF) are suitable. Both cages can be performed with rapid postoperative mobilization and aggressive deformity correction. These cages, unfortunately, can cause lumbar plexus, psoas, bowel, and vascular injuries. The last cage type is Transforaminal Lumbar Interbody Fusion (TLIF). This technique is the best for stabilization and treatment of degenerative lumbar disease following failed conservative treatment (Rahyussalim *et al.*, 2017). Despite the disadvantages, such as paraspinal iatrogenic injury from prolonged muscle retraction, it can still perform direct and unilateral access to the intervertebral foramen and preserve ligamentous structures. This access can reduce direct dissection, the prior chance of damaging back muscles and the thecal sac, minimize bleeding, and improve postoperative recovery (Hammad *et al.*, 2019; Mobbs *et al.*, 2015). The neural foramen is also opened on one side only, so damage to the nerves is less compared to the other technique (Mobbs *et al.*, 2015). With all those advantages, TLIF has become one of the most commonly used techniques for Disc Degeneration Disease treatment and is worth developing.

There is various TLIF spine cage products available on the market. Such as ETurn® TLIF Cage, MediCage®, LOSPA® IS™, and ADONIS®. Even though these implants are already on the market, there are some improvements needed to produce an ideal TLIF spine cage implant. The goal of developing TLIF spine cages is to make an implant that can restore foraminal volume, disc height, sagittal balance, and vertebral alignment. So, the challenges are how to make TLIF spine cages that have a high fusion rate, reduced subsidence, low complications, adjusted to the direction of insertion, are strong enough to endure loads of the lumbar spine, and restore the segment stability by converting distraction force into compression (Walter *et al.*, 2021; Burnard *et al.*, 2020; Peck *et al.*, 2018).

This study aims to improve the TLIF spine cage, which can adjust to the direction and small size of insertion that match the spine size of Indonesian patients. A relatively smaller size might occur due to the morphometry of Indonesians, however, the designed must withstand the body load. This new adjustment was started by observing the morphology of the lumbar spine and adjusting the size with minimum insertion during implantation. A 3D designs of the cage was arranged, and load simulated using finite element method. The finite element analysis was validated by prototyping a 3D printed model as a visual reference and mechanically characterizing it.

2. Methods

2.1. Determining the Size and 3D model of the TLIF Spine Cage

The objective of this study is to realize the cage with Indonesian patients' usage. therefore, we designed the spine cages based on Indonesian Lumbar Morphometry. The morphometry was suggested by Triwidodo *et al.* (2021), which was observed and adapted in current study. The image was then analyzed further using Phyton software to find the specific geometrical parameters (Genisa *et al.*, 2020). Later, a 3D model of TLIF spine cage was realized using Autodesk Inventor Professional 2022 software (San Francisco, California, USA) based on the predetermined size.

The size that needed to determine are the length (L), width (W), height or thickness (H) and lordotic angle (LA). The formulation of L, W, H and LA are explained as followed:

$$L = \frac{60}{100} x\ UVW \quad (1)$$

$$W = \frac{90}{100} x\ PDW \quad (2)$$

$$H = DH \quad (3)$$

$$LA = \arcsin\left(\frac{\frac{PH-PDW}{2}}{\sqrt{(\frac{PH-PDW}{2})^2-(\frac{UVD}{2}^2)}} x\ 2\right) \quad (4)$$

where:

UVW	: upper vertebral width
UVD	: upper vertebral depth
DH	: disc height
PH	: pedicle height
PDW	: pedicle width

The UVW, UVD, DH, PH and PDW will be acquired from obtained data from previous research.

2.2. Prototyping of the TLIF spine scage

In order to execute the 3D design of the spine cage, an additive manufacturing technique commonly known as stereolithography (SLA) was conducted. A Photon Mono X (Anycubic, Shenzhen, China) with LCD-based SLA technology that has faster printing speeds and a larger volume was utilized. The previously determined solid model file in.stl format was now ready to be transferred to the SLA machine. The Photon Mono-X machine uses a bio-photopolymer resin mixed with bio-poly lactic acid from eSUN (Shenzhen, China). The PLA-resin has a low viscosity and has mechanical properties as detailed in Table 1.

Table 1 Mechanical Properties of eResin-PLA at 25˚C

Mechanical Properties	Metrics	Units
Viscosity	200-300	$mPa \cdot s$
Density	1080 – 1130	kg/m^3
Tensile Strength	35-50	Mpa
Flexural Strength	40-60	Mpa
Flexural Modulus	600-800	Mpa
Impact Strength	27 - 40	J/m
Hardness	75 - 80	$Shore\ D$
Elongation at Break	20 - 50	%

2.3. Numerical simulation of TLIF spine cage

A finite element analysis (FEA) was conducted using ANSYS 2022 workbench software (2022 R2 version, Canonsburg, Pennsylvania, USA). In the FEA simulation, the spine cage was assumed to be isotropic (Ahmad *et al.*, 2020). The material that is being simulated for the spine cage is polyetheretherketone (PEEK). The data shows that this material has a compressive strength of 120-300 MPa (depending on the molecular weight) and elongation of a break at around 1.6-43%.

The environmental simulation needed the mechanical properties of the PLA-resin materials. Therefore, a compressive test was conducted to acquire the mechanical parameters of the PLA-resin material. A 3D printed block with the size of 20mm x 10mm x 10mm was prepared as the testing material. The compression was conducted using the universal testing machine MCT-2150 from A&D Company (Tokyo, Japan). The compression rate was set at 10 mm/min.

3. Results and Discussion

3.1. Size Determination and 3D Model of the Spine Cage Implant

There are some parameters from Triwidodo studies that could be considered as important features of the spine cage (Triwidodo *et al.,* 2021). Python image processing is used to sketch the lumbar image, as shown in Figure 1. To name those parameters, were: UVW (upper vertebral width), UVD (upper vertebral depth), DH (disc height), PH (pedicle height), and PDW (pedicle width). The detail of the measurement is shown in Table 1.

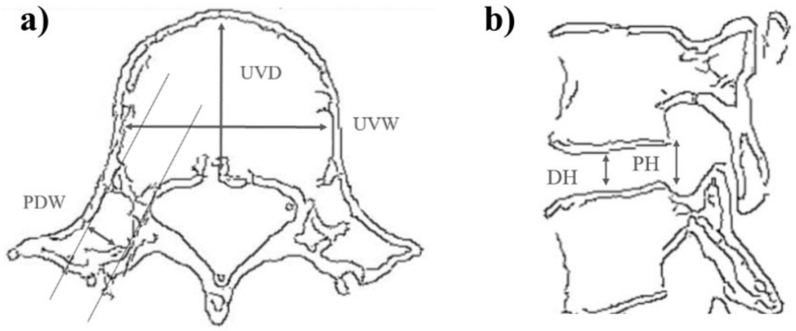

Figure 1 The image processing result of Indonesian Lumbar dimension in sagittal plane (a) and axial plane (b)

Table 1 Lumbar Dimension Indonesian Lumbar dimension in sagittal plane (a) and axial plane (b)

Parameters	Spine Section- L4	Spine Section- L5	Units
UVW	46	48	mm
UVD	33	33	mm
DH	11	10	mm
PH	13	12	mm
PDW	10	13	mm

Spine cage sizes were derived from the dimensions of the above spine section. Note that the spine cage was not designed to cover all the spine areas. The spine cage was designed to be as small as possible compared to that spine section, but the cage must withstand the load from the human body. Based on our study, we converted the dimension of TLIF spine cages to adapt a minimum insertion size at around 8 mm. The formula to calculate the length (L), Width (W), Height (H), and Lordosis Angle (LA) of the TLIF spine cages are given in Equations 1, 2, 3, and 4 based on L4 sizes. The L was calculated to adjust the length area of the cages that can cover the spine area. The W was arranged from the PDW size as the insertion side of the cage. The LA was formulated from the measure of the lordotic angle between two lumbar bodies.

Besides the dimension and angle of the cage, it is known that several factors might influence the biomechanical stability of a lumbar interbody spine cage construct, such as geometry, contact area, and integrated fixation (Triwardono *et al.*, 2021). Therefore, in this paper, we designed a banana-shaped spine cage with a slanted side to facilitate TLIF placement. Based on the lumbar morphometry, formulas, and those biomechanical stability factors, geometry, and sizes of the spine cage design are shown in Table 2.

Table 2 Design Fixture of Spine Cage

Fixture	Metrics	Units
Length	27.7	mm
Width	8	mm
Height	11	mm
Lordosis Angle	7	degree
Jaws Shape	Pyramid	--
Slanted Side	36.5	degree
Window Holes	3	pieces

By following the lumbar morphometry and biomechanical stability factors in Table 2, the TLIF spine cage design is shown in Figure 2. The spine cage consists of a vertical middle hole and two horizontal holes to insert bone graft materials (Figure 2c). The banana-shaped facilitated the placement of the implant through the posterior side. The designed implant has slightly different measurements compare to those available on the market. The length of the designed implant was 27.7 mm and had an angle of 7.27 degrees.

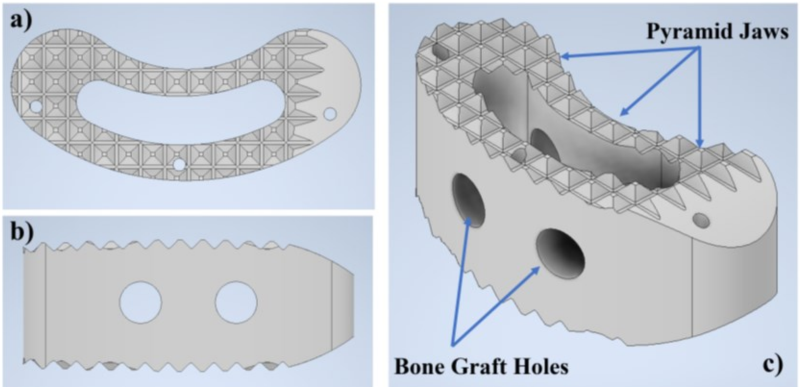

Figure 2 The 3D design of spine cage considering the adjustment of size and features of bone graft holes and pyramid jaws: a) top view; b) side view and perspective view

The fixation for this implant is designed to use a pedicle screw fixation, as an integrated screw fixation is usually not enough to give the biomechanical stability needed for a spine cage implant. For the contact area, the profile of the jaws was made to increase friction and limit the micromotion of the spine cage. Increasing the surface roughness of the spine cage is suitable for fixating the implant to the bone (Triwidodo *et al*., 2021). Therefore, we designed the surface area equipped with a pyramid jaws profile to gain a better osteogenic process. with bone graft than a simple one-type jaws profile design. The pyramid jaws are depicted in Figure 2c.

3.2. Prototyping of the TLIF Spine Cage

The prototyping was conducted using additive manufacturing technology that involves stereolitography of liquid resin. The machine realized the structure as a predetermined design in the 3D model file. The fabrication result was depicted in Figure 3, with an accuracy of around less than 0.5 mm according to the technical specification. Moreover, the realized geometry indicated that the deviation was less than 1 mm compared to the design dimension. It can be concluded that this additive manufacturing technique can be used as a reference model or a prototype of the implant before its transfer to industrial scale. (Syuhada *et al*., 2018).

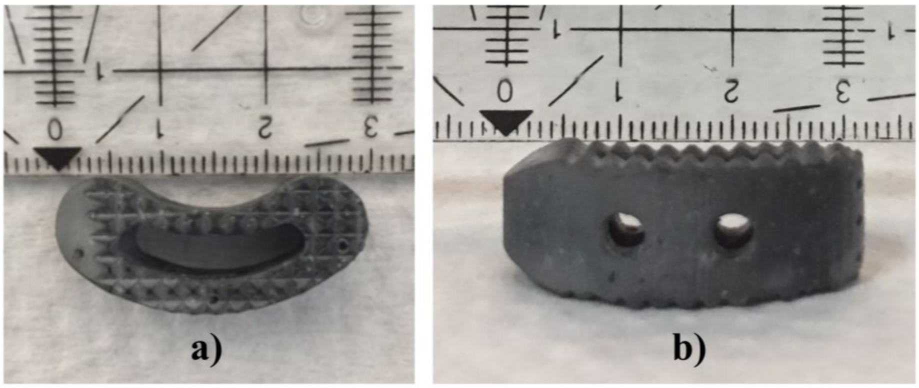

Figure 3 TLIF design printing with PLA Resin: a) top view and b) side view

3.3. Numerical Simulation of TLIF Spine Cage

The numerical simulation predicts that our design would withstand applied loading on the spine cage. The simulation calculates the peak of von Mises stress (PVMS) value as the failure criteria of the selected material of the spine cage (Izmin *et al.*, 2020). Moreover, this study also ensures the safety design of the spine cage with our geometrical arrangement. The stress visualizations of the spine cage simulation are shown in Figure 4. Here, a force of 500 N was applied to the spine cage in an axial direction, following the highest possible loading of the human body (Alief *et al.*, 2019).

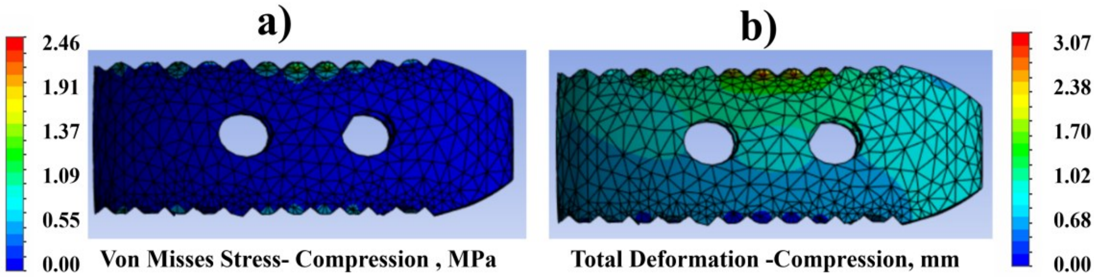

Figure 4 Finite Element Analysis results for spine cage implant: a) Total Deformation - Compression and b) Von Misses – Compression

The simulation results were summarized further in Table 5 to include the maximum point of the spine case during the loading scenario. As shown in Table 5, the von misses results are far below the tensile strength of the simulated material, i.e. PEEK. It suggested that the implant geometry and material successfully support the spinal movement (figure 4a). Also, in torsion and shear simulations, the result does not indicate the failure of the spine cage implant (table 5). A relatively small deformation value from the results also indicate that the implant will be able to function properly (figure 4b). Since compression, tensile, shear, and torsion tests only indicate a simple vertical movement of the spine.

Table 3 Differentiation of Lumbar Interbody Fusion Implant

Design	Von misses (MPa)	Total deformation (mm)	Tensile strength (MPa)	Shear Stress (MPa)	Maximum Shear Stress (MPa)	Torsion (MPa)	Maximum torsion (MPa)
Spine Cage	0.117	± 0.758	35 – 50	1.99×10^{-2}	3.37	$3{,}15 \times 10^{-3}$	$5{,}7 \times 10^{-2}$

3.4. Validation of the model

A comparison of numerical simulation and the experimental setup is needed to validate the numerical study in our previous section. We simulate a compressive test of the realized resin-PLA spine cage in the finite element environment. This phenomenon was followed by compression using the universal testing machine. Figure 5 shows the Finite Element Analysis of the sample block in terms of its total deformation and calculated von Misses Stress.

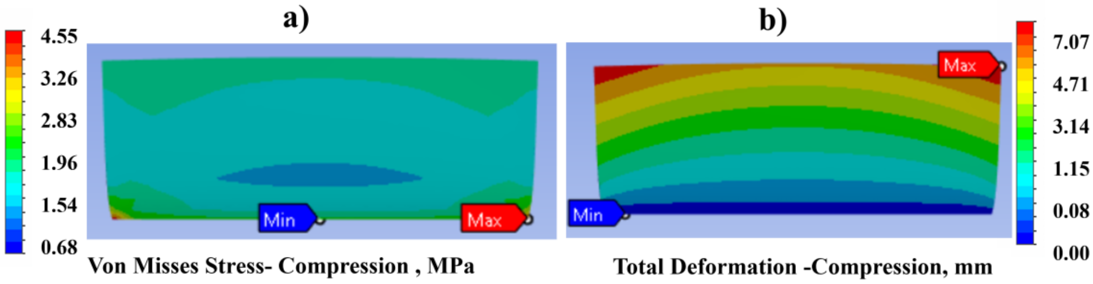

Figure 5 Finite Element Analysis results for PLA sample block: a) Von Misses and b) total deformation in compression testing mode

The compressive test on a 3D printed acquire the young's modulus value at around 55.6 MPa. This value was confirmed by our previous study (Supriadi *et al.*, 2021, Saseendran *et al.*, 2017). A 500 N vertical compression and tensile force were given from the top surface to calculate Von Mises and deformation of the implant (He *et al.*, 2021). Shear stress with 200 N and 25 Nm torsion was also evaluated in this implant simulation (Krijnen *et al.*, 2006; Pitzen *et al.*, 2000). Table 4 shows the mechanical parameters in the Ansys simulation software.

Table 4 Parameters for Finite Element Analysis

Density (g/mm3)	Young's Modulus (MPa)	Poisson's Ratio	Reference
1.13	55.6	0.35	(Saseendran *et al.*, 2017)

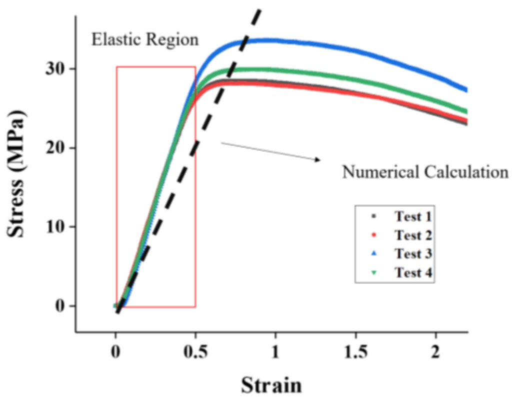

Figure 6 Compressive test result for PLA sample block compare with the numerical calculation of elastic modulus

Figure 6 presents the experimental result of block test (with four repetitions of samples). It showed its maximum strength at around 30 MPa. The numerical simulation gives the dotted line in Figure 6. The line was projected from the force-displacement relation from the environmental simulation (Figure 5). It showed a deviation of 9% compared to the experimental result. Consequently, it can be suggested that the simulation result of spine cage has a 9% gap mostly in the elastic region (red line area in Figure 6).

4. Conclusions

A TLIF spine cage based on Indonesian morphometry with a 28 x 9 x 11 mm dimension was designed with a pyramid-shaped jaw profile, multiple holes as a space for bone graft, and a thread hole for insertion of the implant into the disc space. We performed a finite element analysis simulation with the Ansys software, performing compression and tensile tests to stimulate the stress impacted on the implant. Shear and torsion test was also simulated in this research. This simulation was done to test the strength of the design using PLA Resin material. The results showed that the design is strong enough to withstand the force given. Our numerical study also showed that a deviation around 9% between experimental loading and numerical calculation might occurred. However, it is believed that this gap between experimental and realization might give important information when the candidate material, PEEK, will be used in the future application.

Acknowledgments

The authors would like to acknowledge the Matching Fund Grant No.279/PKS/WRIII-DISTP/UI/2022 from Kementerian Pendidikan, Kebudayaan, Riset, dan Teknologi.

References

Ahmad, M.A., Zulkifli, N.N.M.E., Shuib, S., Sulaiman, S.H., Abdullah, A.H., 2020. Finite Element Analysis of Proximal Cement Fixation in Total Hip Arthroplasty. *International Journal of Technology*, Volume 11(5), pp. 1046–1055

Alief, N.A., Supriadi, S., Whulanza, Y., 2019. Modelling The Shape Memory Properties of 4D Printed Polylactic Acid (PLA) for Application of Disk Spacer in Minimally Invasive Spinal Fusion. *In*: AIP Conference Proceedings, 2092, 020005

Burnard, J.L., Parr, W.C.H., Choy, W.J., Walsh, W.R., Mobbs, R.J., 2020. 3D-printed Spine Surgery Implants: A Systematic Review of The Efficacy and Clinical Safety Profile of Patient-Specific and Off-The-Shelf Devices. *European Spine Journal*, Volume 29(6), pp. 1248–1260

Genisa, M., Shuib, S., Ahmad Rajion, Z.A., Mohamad, D., Arief, M.E., 2020. Dental Implant Monitoring Using Resonance Frequency Analysis (RFA) and Cone Beam Computed Tomography (CBCT) Measurement. *International Journal of Technology*, Volume 11(5), pp. 1015–1024

Hammad, A., Wirries, A., Ardeshiri, A., Nikiforov, O., Geiger, F., 2019. Open Versus Minimally Invasive TLIF: Literature Review and Meta-Analysis. *Journal of Orthopaedic Surgery and Research*, Volume 14(1), p. 229

He, L., Xiang, Q., Yang, Y., Tsai, T.Y., Yu, Y., Cheng, L., 2021. The Anterior and Traverse Cage Can Provide Optimal Biomechanical Performance for Both Traditional and Percutaneous Endoscopic Transforaminal Lumbar Interbody Fusion. *Computers in Biology and Medicine*, Volume 131, p. 104291

Hennemann, S., de Abreu, M.R., 2021. Estenose Degenerativa Do Canal Lombar (*Degenerative Stenosis of The Lumbar Canal*). *Revista Brasileira de Ortopedia*, Volume 56(01), pp. 009–017

Izmin, N.A.N., Hazwani, F., Todo, M., Abdullah, A.H., 2020. Risk of Bone Fracture in Resurfacing Hip Arthroplasty at Varus and Valgus Implant Placements. *International Journal of Technology*, Volume 11(5), pp. 1025–1035

Krijnen, M.R., Mensch, D., van Dieen, J.H., Wuisman, P.I., Smit, T.H., 2006. Primary Spinal Segment Stability with a Stand-Alone Cage: In Vitro Evaluation of a Successful Goat Model. *Acta Orthopaedica*, Volume 77(3), pp. 454–461

Lee, B.H., Moon, S.H., Suk, K.S., Kim, H.S., Yang, J.H., Lee, H.M., 2020. Lumbar Spinal Stenosis: Pathophysiology and Treatment Principle: A Narrative Review. *Asian Spine Journal*, Volume 14(5), pp. 682–693

Mobbs, R.J., Phan, K., Malham, G., Seex, K., Rao, P.J., 2015. Lumbar Interbody Fusion: Techniques, Indications and Comparison of Interbody Fusion Options Including PLIF, TLIF, MI-TLIF, OLIF/ATP, LLIF and ALIF. *Journal of Spine Surgery*, Volume 1(1), pp. 2–18

Peck, J.H., Kavlock, K.D., Showalter, B.L., Ferrell, B.M., Peck, D.G., Dmitriev, A.E., 2018. Mechanical Performance of Lumbar Intervertebral Body Fusion Devices: An Analysis of Data Submitted to The Food and Drug Administration. *Journal of Biomechanics*, Volume 78, pp. 87–93

Pitzen, T., Geisler, F.H., Matthis, D., Müller-Storz, H., Steudel, W.I., 2000. Motion of Threaded Cages in Posterior Lumbar Interbody Fusion. *European Spine Journal*, Volume 9(6), pp. 571–576

Rahyussalim, A.J. Kurniawati, T., Aprilya, D., Anggraini, R., Ramahdita, G., Whulanza, Y., 2017. Toxicity and Biocompatibility Profile of 3D Bone Scaffold Developed by Universitas Indonesia: A Preliminary Study. *AIP Conference Proceedings*, Volume 1817, p. 020004

Saseendran, S., Wysocki, M., Varna, J., 2017. Cure-state Dependent Viscoelastic Poisson's Ratio of LY5052 Epoxy Resin. *Advanced Manufacturing: Polymer & Composites Science*, Volume 3(3), pp. 92–100

Supriadi, S., Rachman, P., Saragih, A.S., Whulanza, Y., Rahyussalim, A.J., Triwidodo, A., 2021. Design, Development, and Finite Element Study on The Novel Biomimetic Lumbosacroiliac Prosthesis. In: *AIP Conference Proceedings*, AIP Publishing LLC, Volume 2344(1), p. 050021

Syuhada, G., Ramahdita, G., Rahyussalim, A.J., Whulanza, Y. Multi-material Poly (Lactic Acid) Scaffold Fabricated Via Fused Deposition Modeling and Direct Hydroxyapatite Injection as Spacers in Laminoplasty. *AIP Conference Proceedings*, Volume 1933, p. 020008

Triwidodo, A., Rahyussalim, A.J., Yulisa, N.D., Pandelaki, J., Huraiby, L.S., Hadi, I.A.N., Liosha, F.Y., Dilogo, I.H., 2021. Sacrum Morphometry and Spinopelvic Parameters Among The Indonesian Population Using Computed Tomography Scans. *Medicine*, Volume 100(47)

Triwardono, J., Supriadi, S., Whulanza, Y., Saragih, A.S., Novalianita D.A., Utomo, M.S., Kartika, I., 2021. Evaluation of The Contact Area in Total Knee Arthroplasty Designed for Deep Knee Flexion. *International Journal of Technology,* Volume 12(6), pp. 1312–1322

Walter, C., Baumgärtner, T., Trappe, D., Frantz, S., Exner, L., Mederake, M., 2021. Influence of Cage Design on Radiological and Clinical Outcomes in Dorsal Lumbar Spinal Fusions: A Comparison of Lordotic and Non-Lordotic Cages. *Orthopaedic Surgery*, Volume 13(3), pp. 863–875